MULTISCALE MODELING OF IMPACT BEHAVIOR FOR POLYMER COMPOSITES

Harpreet Singh[1], Mohit Gupta[1], Puneet Mahajan[1]

[1]Department of Applied Mechanics, Indian Institute of Technology Delhi,
New Delhi, Delhi 110016, India. Phone: +91 11 26591229,
Email: composites.impact@gmail.com

Keywords– Multiscale model, Asymptotic expansion homogenization (AEH), Reduced order modeling, Low Velocity Impact (LVI), Epoxy plasticity

Abstract

Asymptotic expansion homogenization is a well proven technique for analyzing the behavior of periodic structures which has been widely being used for fiber reinforced composites. The present paper discusses about multiscale formulation based on asymptotic homogenization method for modeling the inelastic deformations (plasticity and damage) of matrix (epoxy). The multiscale framework using reduced order modeling provides the benefit of reducing the computational cost. Properties of epoxy are determined experimentally and mimicked numerically by using plasticity based material models. Proposed model is then validated with the low velocity impact experiments of E-glass epoxy composite. Proposed model shows the capability of capturing contact force and energy time histories.

1 INTRODUCTION

Fiber-reinforced composites are heterogeneous materials where the heterogeneities in form of long fibers embedded in the matrix (epoxy-commonly used). The complex hierarchical micro-structure causes the load response of these materials very difficult to predict. RVE based analysis for effective property determination involves two different scales i.e. the macroscopic scale where the domain is regarded as homogeneous and heterogeneities are not visible, second is microscopic scale which is called as scale of heterogeneity. Multi-scale modeling for the heterogeneous materials is based on the concept of obtaining and passing the information from one scale to another scale which starts from lower most scale at which material data for its constituents are easily determinable. This data is used to determine the load-response information which is passed to next scale. For fiber-reinforced composites, a RVE is generated at microscale which represents the basic fiber-matrix structure, at each Gauss point in the finite elements constituting the domain. An asymptotic expansion homogenisation procedure is adopted to determine the load-response information in the form of various functions such as elastic influence functions and damage influence functions. These functions collectively represent the behavior of the material at next scale. For two-scale formulation of fiber-reinforced composites, the next scale is regarded as scale of lamina or macroscale. The homogenized properties at lamina-scale are represented as the functions of these influence functions and the macroscale stress-strain response can be represented in terms of these homogenized material data. Based on the mentioned procedure, section 2 explains the procedure to determine the homogenized properties and the method to obtain macroscale stress-strain response using the homogenized properties. The damage and plasticity induced effects at microscale can be devised in the form of eigen strains as explained in section 3 and 4. Section 5 and 6 explains about the low velocity impact experiments and conducted simulations to validate the experimental data respectively.

2 DETERMINATION OF HOMOGENIZED PROPERTIES

Let us consider a composite material consisting of a domain, $\mathscr{X}$. The statistically homogeneous RVE is denoted as $\mathscr{Y}$ which consists of multiple materials. Let $\mathbf{x}$ be a position vector defined at macroscale, $\mathscr{X}$. Similarly $\mathbf{y}$ is the position vector defined at microscale, $\mathscr{Y}$. ξ, a positive number denotes the scale factor and is defined as the ratio of macroscale dimension, $\mathbf{x}$ to microscale dimension, $\mathbf{y}$.

Two scale ($\mathscr{X} \times \mathscr{Y}$) asymptotic expansion homogenization (AEH) procedure can be adopted to get the macroscopic response using the microscopic details and properties. The advantage of AEH methodology is that it enables the macroscopic properties to be calculated in terms of some characteristic microscale functions which are termed as influence functions. Using this method the response functions at the global or macroscale can be represented as

$$u_i^{\xi}(\mathbf{x}) = u_i^{(0)}(\mathbf{x},\mathbf{y}) + \xi u_i^{(1)}(\mathbf{x},\mathbf{y}) + \xi^2 u_i^{(2)}(\mathbf{x},\mathbf{y}) + \cdots \tag{1}$$

$$\varepsilon_{ij}^{\xi}(\mathbf{x}) = \xi^{(-1)}\varepsilon_{ij}^{(-1)}(\mathbf{x},\mathbf{y}) + \varepsilon_{ij}^{(0)}(\mathbf{x},\mathbf{y}) + \xi\varepsilon_{ij}^{(1)}(\mathbf{x},\mathbf{y}) + \xi^2\varepsilon_{ij}^{(2)}(\mathbf{x},\mathbf{y}) + \cdots \tag{2}$$

$$\sigma_{ij}^{\xi}(\mathbf{x}) = \xi^{(-1)}\sigma_{ij}^{(-1)}(\mathbf{x},\mathbf{y}) + \sigma_{ij}^{(0)}(\mathbf{x},\mathbf{y}) + \xi\sigma_{ij}^{(1)}(\mathbf{x},\mathbf{y}) + \xi^2\sigma_{ij}^{(2)}(\mathbf{x},\mathbf{y}) + \cdots \tag{3}$$

$$\mu_{ij}^{\xi}(\mathbf{x}) = \mu_{ij}^{(0)}(\mathbf{x},\mathbf{y}) + \xi\mu_{ij}^{(1)}(\mathbf{x},\mathbf{y}) + \xi^2\mu_{ij}^{(2)}(\mathbf{x},\mathbf{y}) + \cdots \tag{4}$$

where $u_i^{(s)}(\mathbf{x},\mathbf{y})$, $\varepsilon_{ij}^{(s-1)}(\mathbf{x},\mathbf{y})$, $\sigma_{ij}^{(s-1)}(\mathbf{x},\mathbf{y})$ and $\mu_i^{(s)}(\mathbf{x},\mathbf{y})$ with $s \in \mathbb{N}$, are the periodic functions in microscale. The macroscopic eigen strain, $\mu_{ij}(\mathbf{x},\mathbf{y})$ depends upon the material properties of each phase i.e. fiber, matrix and interphase constitutive behavior and state variable, ϕ. Now using Eq.(1), Eq.(2), Eq.(3) and Eq.(4), the equilibrium equations at microscale can be expressed as following:

$$\mathscr{O}(\xi^{-2}) \qquad \frac{\partial \sigma_{ij}^{(-1)}}{\partial y_j} = 0 \tag{5}$$

$$\mathscr{O}(\xi^{-1}) \qquad \frac{\partial \sigma_{ij}^{(0)}}{\partial y_j} + \frac{\partial \sigma_{ij}^{(-1)}}{\partial x_j} = 0 \tag{6}$$

$$\mathscr{O}(\xi^{0}) \qquad \frac{\partial \sigma_{ij}^{(0)}}{\partial x_j} + \frac{\partial \sigma_{ij}^{(1)}}{\partial y_j} + f_i = 0 \tag{7}$$

Considering $\mathscr{O}(\xi^{-2})$ term first; multiply Eq.(5) with $u_i^{(0)}$ and integrating by parts gives

$$u_i^{(0)} = u_i^{(0)}(\mathbf{x}) \tag{8}$$

$$\sigma_{ij}^{(-1)}(\mathbf{x},\mathbf{y}) = 0 \tag{9}$$

Let us take $\mathscr{O}(\xi^{-1})$ term (Eq.(6))

$$\sigma_{ij,y_j}^{(0)} = 0 \tag{10}$$

Eq.(10) can be expressed as

$$\left\{ L_{ijkl}^{\xi}(\mathbf{y}) \left(\frac{\partial u_k^{(0)}}{\partial x_l} + \frac{\partial u_k^{(1)}}{\partial y_l} - \mu_{kl}^{(0)}(\mathbf{x},\mathbf{y}) \right) \right\}_{,y_j} = 0 \tag{11}$$

Using the fact that the term $\frac{\partial u_k^{(0)}}{\partial x_l}$ is a constant w.r.t. operator '$,y_j$', the first order deformation can be represented in terms of macroscale strain and eigen strain as

$$u_i^{(1)}(\mathbf{x},\mathbf{y}) = H_i^{kl}(\mathbf{y}) u_{k,x_l}^{(0)}(\mathbf{x}) + \int_{\mathscr{Y}} \chi_i^{kl}(\mathbf{y},\tilde{\mathbf{y}}) \mu_{kl}^{(0)}(\mathbf{x},\tilde{\mathbf{y}})\, d\tilde{\mathscr{Y}} \tag{12}$$

where H_i^{kl} and χ_i^{kl} are transformation tensors that relate the first order displacement to macroscale strain and eigen strain respectively. The computational cost can be made affordable by subdividing the domain into finite number of sets which results in reduction of the order of microscale domain. So the weighted average of response functions over these sub-domains represents the the response of RVE. Based on this, the eigen strain, $\mu^{(0)}$can be defined as

$$\mu_{ij}^{(0)}(\mathbf{x},\mathbf{y}) = \sum_{\alpha=1}^{M} N^{(\alpha)}(\mathbf{y})\mu_{ij}^{(\alpha)}(\mathbf{x}) \tag{13}$$

where α designates a particular set and M denotes the finite number of sets which are used to represents the response of microstructure. The eigen strains may be discontinuous across these sub-domains and have $\mathscr{C}^{-1}(\mathscr{Y})$ continuity. The functions $N^{(\alpha)}$ are also assumed to follow the condition of partition of unity. The choice regarding the shape functions is further simplified by using the following:

$$N^{(\alpha)}(\mathbf{y}) = \begin{cases} 1 & \mathbf{y} \in \mathscr{Y}^{(\alpha)} \\ 0 & \mathbf{y} \notin \mathscr{Y}^{(\alpha)} \end{cases} \tag{14}$$

Using Eq.(12) and Eq.(14), Eq.(11) can be simplified by writing it for particular sub-domain

$$\left\{ L_{ijkl}(\mathbf{y}) \left(\left[I_{klmn} + \frac{\partial H_k^{mn}}{\partial y_l} \right] \frac{\partial u_m^{(0)}}{\partial x_n} + \int_{\mathscr{Y}^{(\alpha)}} \frac{\partial \chi_k^{mn}(\mathbf{y},\tilde{\mathbf{y}})}{\partial y_l} d\tilde{\mathscr{Y}}^{(\alpha)} \mu_{mn}^{(\alpha)}(\mathbf{x}) - \mu_{kl}^{(\alpha)}(\mathbf{x}) \right) \right\}_{,y_j} = 0 \tag{15}$$

The two cases i.e. (1).$\frac{\partial u_m^{(0)}}{\partial x_n} \neq 0$ where as $\mu_{mn}(\mathbf{x}) = 0$ and (2). $\frac{\partial u_m^{(0)}}{\partial x_n} = 0$ where as $\mu_{mn}(\mathbf{x}) \neq 0$ represent two distinct boundary value problems which can be used to calculate H_k^{mn} and χ_k^{mn}.

Using Eq.(12) and Eq.(13), $\varepsilon_{ij}^{(0)}(\mathbf{x},\mathbf{y})$ can be expressed as

$$\varepsilon_{ij}^{(0)}(\mathbf{x},\mathbf{y}) = \left[I_{ijkl} + H_{i,y_j}^{kl}(\mathbf{y}) \right] u_{k,x_l}^{(0)}(\mathbf{x}) + \int_{\mathscr{Y}} \chi_{i,y_j}^{kl}(\mathbf{y},\tilde{\mathbf{y}}) \sum_{\alpha=1}^{M} N^{(\alpha)}(\mathbf{y})\mu_{kl}^{(\alpha)}(\mathbf{x})\, d\tilde{\mathscr{Y}} \tag{16}$$

After rearrangement, $\varepsilon_{ij}^{(0)}(\mathbf{x},\mathbf{y})$ can also be averaged over each sub-domain $\mathscr{Y}^{(\beta)}$ which gives

$$\varepsilon_{ij}^{(0)^{(\beta)}}(\mathbf{x}) = E_{ijkl}{}^{(\beta)} \frac{\partial u_k^{(0)}}{\partial x_l} + \sum_{\alpha=1}^{M} S_{ijkl}{}^{(\alpha\beta)} \mu_{kl}^{(\alpha)}(\mathbf{x}) \tag{17}$$

where

$$E_{ijkl}{}^{(\beta)} = I_{ijkl} + \frac{1}{\mid \mathscr{Y}^{(\beta)} \mid} \int_{\mathscr{Y}^{(\beta)}} H_{i,y_j}^{kl}\, d\mathscr{Y}^{(\beta)} \tag{18}$$

and

$$S_{ijkl}{}^{(\alpha\beta)} = \frac{1}{\mid \mathscr{Y}^{(\beta)} \mid} \int_{\mathscr{Y}^{(\beta)}} S_{ijkl}^{(\alpha)}\, d\mathscr{Y}^{(\beta)} \tag{19}$$

Macroscopic stress can be calculated by volume averaging of leading order term only:

$$\sigma_{ij}^{\mathscr{X}}(\mathbf{x}) = \frac{1}{\mid \mathscr{Y} \mid} \int_{\mathscr{Y}} \sigma_{ij}^{(0)}(\mathbf{x},\mathbf{y})\, d\mathscr{Y} \tag{20}$$

Using Eq.(17), Eq.(20) can be expressed as

$$\boxed{\sigma_{ij}^{\mathscr{X}}(\mathbf{x}) = \bar{L}_{ijpq}\varepsilon_{pq}^{\mathscr{X}}(\mathbf{x}) + \sum_{\alpha=1}^{M} \bar{M}_{ijpq}^{(\alpha)}\mu_{pq}^{(\alpha)}(\mathbf{x})} \tag{21}$$

where

$$\bar{L}_{ijpq} = \frac{1}{\mid \mathscr{Y} \mid} \int_{\mathscr{Y}} L^{\xi}_{ijkl}(\mathbf{y}) E_{klpq}(\mathbf{y})\, d\mathscr{Y} \qquad \bar{M}^{(\alpha)}_{ijpq} = \frac{1}{\mid \mathscr{Y} \mid} \int_{\mathscr{Y}} L^{\xi}_{ijkl}(\mathbf{y}) \left(S^{(\alpha)}_{klpq}(\mathbf{y}) - I_{klpq} \right) d\mathscr{Y} \tag{22}$$

Eq.(17) shows the nonlinear system of equations which is written in incremental form. Further $\Delta\mu_{ij}$ for a particular subdomain α depends upon $\Delta\varepsilon_{ij}$ as per following constitutive relation. The subscript (α) is omitted further for the sake of clarity:

$$\Delta\mu_{ij} = \Delta\varepsilon_{ij} - L^{-1}_{pqij}\Delta\sigma_{pq} \tag{23}$$

In the derivative form Eq.(23) is written as

$$\frac{\partial\Delta\mu_{ij}}{\partial\Delta\varepsilon_{kl}} = I_{ijkl} - L^{-1}_{pqij}\frac{\partial\Delta\sigma_{pq}}{\partial\Delta\varepsilon_{kl}} \tag{24}$$

The tangent stiffness, $\frac{\partial\Delta\sigma_{ij}}{\partial\Delta\varepsilon_{kl}}$ depends upon the state of the material which further depends upon plastic strains and damage at any location in the material. For calculating the damage induced eigen strain, μ_{ij} a damage variable, Ω is defined as per continuum damage mechanics theory. Let $\mathbf{L}^{ep}$ is the stiffness of the material which includes the plastic behavior. $\mathbf{L}^{o}$ denotes the stiffness of undamaged material. Actual stress, σ at any material point can be expressed incrementally as;

$$\Delta\sigma_{ij} = \Delta L_{ijkl}\varepsilon^{e}{}_{kl} + L_{ijkl}\Delta\varepsilon^{e}{}_{kl} \tag{25}$$

or

$$\Delta\sigma_{ij} = \left(\frac{\Delta L_{ijkl}}{\Delta\varepsilon^{e}_{pq}}\varepsilon^{e}_{kl} + L_{ijpq} \right) \Delta\varepsilon^{e}{}_{pq} \tag{26}$$

Finally

$$\frac{\partial\Delta\sigma_{ij}}{\partial\Delta\varepsilon_{tu}} = \left(\frac{\Delta L_{ijkl}}{\Delta\varepsilon^{e}_{pq}}\varepsilon^{e}_{kl} + L_{ijpq} \right) (L^{o})^{-1}_{rspq} L^{ep}_{rstu} \tag{27}$$

Now $\left(\frac{\Delta L_{ijkl}}{\Delta\varepsilon^{e}_{pq}}\right)$ can be calculated as

$$\left(\frac{\Delta L_{ijkl}}{\Delta\varepsilon^{e}_{pq}} \right) = \left(\frac{\Delta L_{ijkl}}{\Delta\Omega} \right) \left(\frac{\Delta\Omega}{\Delta\varepsilon^{e}_{pq}} \right) \tag{28}$$

The value of $\left(\frac{\Delta\Omega}{\Delta\varepsilon^{e}_{pq}}\right)$ depends further upon the variation of damage with respect to strain.

3 MATERIAL MODELS FOR THE CONSTITUENTS

In current work the unit cell of 50.6% volume fraction containing single fiber in the center and an elasto-plastic epoxy surrounding it with perfectly bonded interface is considered. Glass fibers are modeled elastic and a brittle damage is assumed. The experimental data shows that epoxy resin behaves in ductile manner but differently under compressive and tensile load. The same behavior can be mimicked numerically using a hydrostatic pressure dependent quadratic yield function. These kind of yield functions have been used by many other researchers [1, 2, 3] to describe the experimentally observed response of the epoxy resin. Yield surface, as proposed by [1] for polymer resins, is adopted for present study. This can be represented as

$$f = \frac{1}{2}\left[(\sigma_1 - \sigma_2)^2 + (\sigma_2 - \sigma_3)^2 + (\sigma_3 - \sigma_1)^2 \right] + (Y_c - Y_t)\left[\sigma_1 + \sigma_2 + \sigma_3\right] - Y_c Y_t \tag{29}$$

where σ_1, σ_2, σ_3 are principal stresses. Y_c and Y_t denotes the absolute values of compressive and tensile yield strengths. The quantity $(\sigma_1 + \sigma_2 + \sigma_3)$ includes the effect of applied hydrostatic pressure which vanishs in case of $Y_c = Y_t$.

The incremental plastic strains are calculated using a non-associated flow rule. The plastic potential function for this purpose is assumed as following

$$g = \frac{1}{2}\left[(\sigma_1 - \sigma_2)^2 + (\sigma_2 - \sigma_3)^2 + (\sigma_3 - \sigma_1)^2\right] + \beta\,(Y_c - Y_t)\,[\sigma_1 + \sigma_2 + \sigma_3] \tag{30}$$

where β is a constant and the value of this constant is determined by reproducing the experimental stress-strain data for both uniaxial tension and compression. It is also ensured that the plastic Poisson's ratio, ν_p should always be less than 0.5. Following relation determines the value of β from uniaxial tension test condition:

$$\beta = \frac{3p}{Y_c - Y_t}\left(\frac{1 - 2\nu_p}{1 + 2\nu_p}\right) \tag{31}$$

where p is applied hydrostatic pressure.

Cracks in the material causes the softening of material which can be quantified using continuum damage mechanics based framework. First for the initiation of damage in the polymer matrix or fibers, a maximum strain based criteria is used which is represented as

$$\left\|\varepsilon_{ij}\right\| = \max[\varepsilon_{ij}] \geq \varepsilon^f \tag{32}$$

where ε^f is the failure strain and determined from experimental uniaxial tension conditions. The effect of damage growth in terms of reduction in stiffness can be accounted using a damage variable, Ω. The scalar damage variable, Ω can be calculated by using an exponential function proposed by [4] which can be expressed as

$$\Omega = 1 - exp\left(\frac{-1}{me}\left(\frac{\left\|\varepsilon_{ij}\right\|}{\varepsilon^f}\right)^m\right) \tag{33}$$

where m is the material constant which can be calculated experimentally for each phase. e is Napier's constant.

4 MATERIAL CHARACTERIZATION OF THE CONSTITUENTS

4.1 Material characterization of glass fiber

The unidirectional E-glass fabric of 580 GSM used in the present work was purchased from Saertex. The average diameter of the fibers measured over 5 samples was 17 micro-meter. The following material data [5] as shown in Tab.1 is used in the present study.

Table 1: Glass fiber material properties ([5])

Material Property	Value
Breaking Strength	2035.95 MPa
Tensile Failure Strain	0.0224

4.2 Material characterization of epoxy

The epoxy system used for preparing samples was Epikote RIMR 135 resin and RIMH 134 hardener which were mixed in the ratio of 100:30 parts by weight. This particular epoxy system was selected as

it has low viscosity and suitable for composite manufacturing by vacuum infusion process (VARIM). To evaluate the damage growth and plastic strains in epoxy under tension and compression loading, load-unload tests were performed using cylindrical specimens. Tension specimens dimensions were referred from [6] and length to width ratio was kept similar with diameter 6 mm. Compression standard specimens were prepared as per ASTM D695-10 with height to diameter ratio kept 1 in order to avoid buckling of specimens.

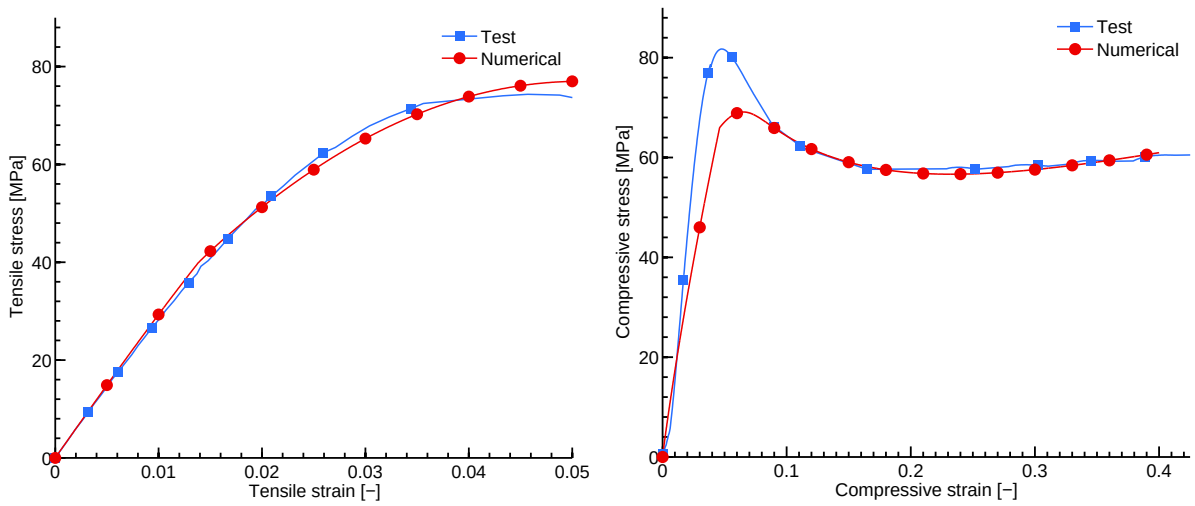

(a) (b)

Figure 1: Comparison of experimental and numerical stress strain data for epoxy under (a) Tension and (b) Compression

Tension tests were performed at 1 mm/min to obtain longitudinal and transverse strains. Four load unload cycles were performed in a displacement control mode with a cross-head speed of 1mm/min. Plastic strains were calculated by extending the straight lines joining peak and bottom points of every cycle. Slope of these straight lines gave the damaged modulus and hence the growth of damage variable was captured/evaluated. Compression tests at a rate of 3mm/min were conducted by placing the cylindrical pure epoxy sample between the flat plates. The recorded experimental data for tension and compression is simulated numerically by using the material model as described in section 3. Elastic moduli for tension and compression are calculated from the initial slopes of experimental stress-strain curves. Initial yield strength values, $Y_c^{(o)}$ = 67 MPa and $Y_t^{(o)}$ = 45 MPa are determined at 0.2 % strain offset. As shown in Fig. 1a and 1b by reproducing the experimental data using eq. (29), (30) and (33), the values of parameters such as β, m and ε_f are determined.

5 IMPACT TESTING FOR MACROSCALE VALIDATIONS

5.1 Drop-weight impact (Low Velocity Impact - LVI) test

For conducting the impact tests, laminated E-glass/epoxy composite panels about 400 mm $\times$ 400 mm in size were prepared using vacuum assisted resin infusion molding (VARIM) process. 175 mm $\times$ 175 mm plates were cut from these panels and each plate had 8 layers of glass fiber in layup sequence $[0/90/0/90]_s$. Drop weight impact tests were performed in accordance with the method prescribed in ASTM D7136 for measuring the impact resistance of a fibre-reinforced polymer (FRP) composite using a fully instrumented INSTRON Dynatup 9250 HV drop tower as shown in Fig. 2. The rectangular specimen was subjected to an out-of-plane impact (perpendicular to the plane of the laminate) using

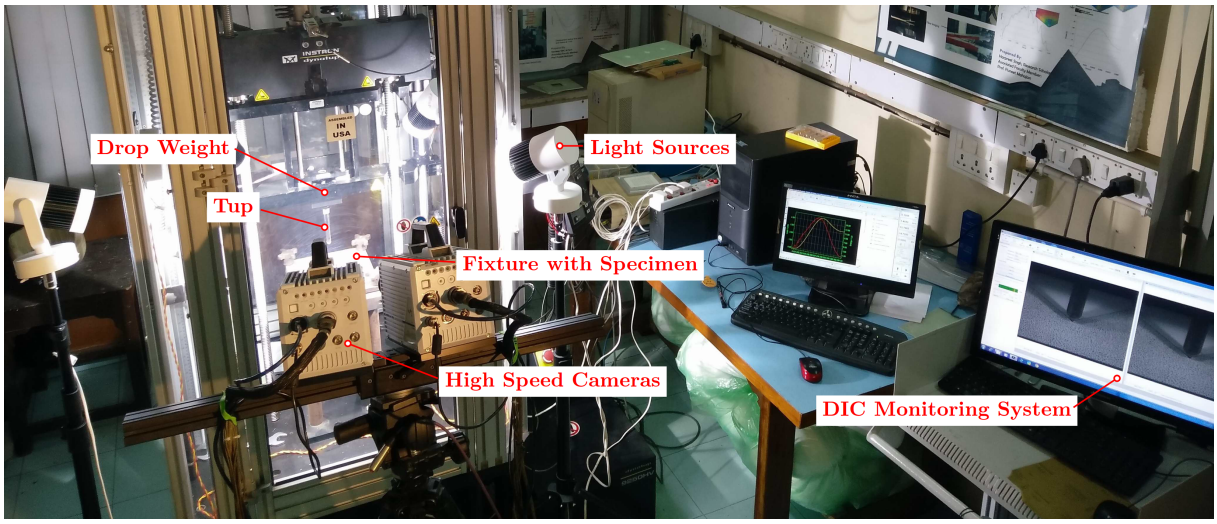

Figure 2: Experimental drop test setup with DIC monitoring system

a drop-weight device with a hemispherical striker tup of mass 13 kg, diameter Φ12.7 mm and initial velocity of 1.25 m/s. The specimen was placed in the rigid fixture and securely fixed using four screw clamps between upper and lower frame which resulted an open effective area of 125 mm × 125 mm. The drop-weight impact device utilized along with DIC setup is shown in Fig. 2. The impact force as function of the contact time, t, was recorded digitally by reading the output of a load-cell installed inside the impactor tup.

6 MULTISCALE SIMULATIONS AND VALIDATION WITH EXPERIMENTS

To validate the proposed multiscale formulation, a user defined subroutine VUMAT is developed for the constitutive model in ABAQUS/Explicit. A FE model is generated which includes a composite plate, steel fixture frame and impactor geometries. These solid bodies are meshed with C3D8, full

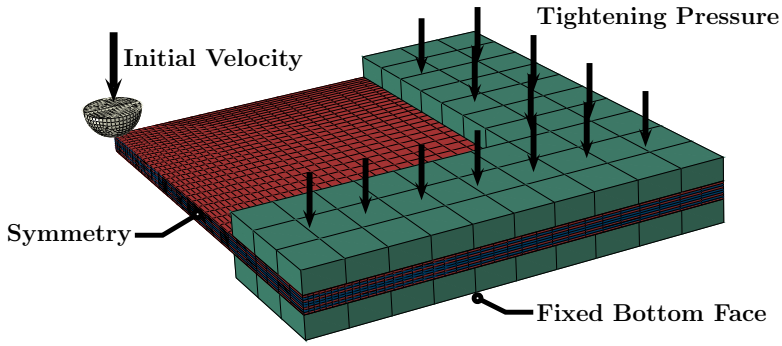

Figure 3: Equivalent quarter FE model labeled with boundary and loading conditions

integration linear elements except impactor which is assumed as rigid body. Taking the geometrical configuration and loading conditions into consideration, quarter symmetry is used in simulation to reduce the computational time. Single element across the thickness is taken each ply. Impactor is modeled as hemi-sphere with 13 kg mass and Φ12.7 mm diameter. The preload applied on the frame for tightening the plate is modeled as equivalent pressure applied at the top face. Bottom face of the frame is fixed in all

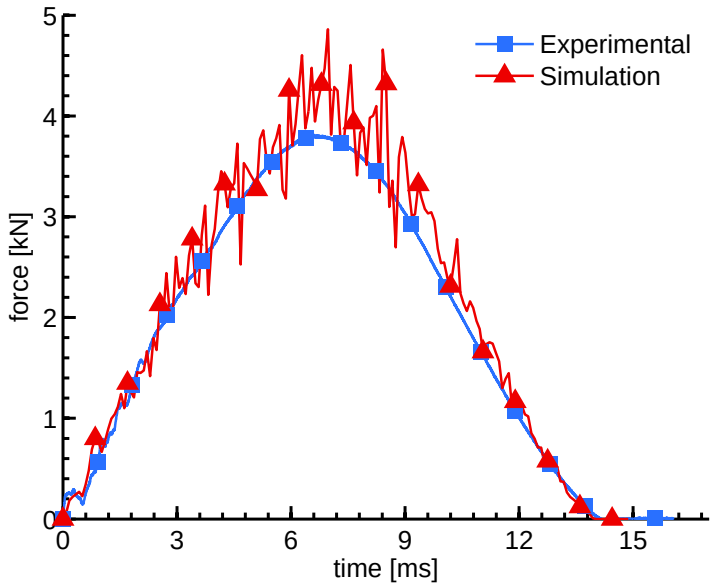

Figure 4: Variation of contact force with time in experiment and simulation

directions. To simulate the interlaminar damage, ABAQUS inbuilt traction-displacement based cohesive

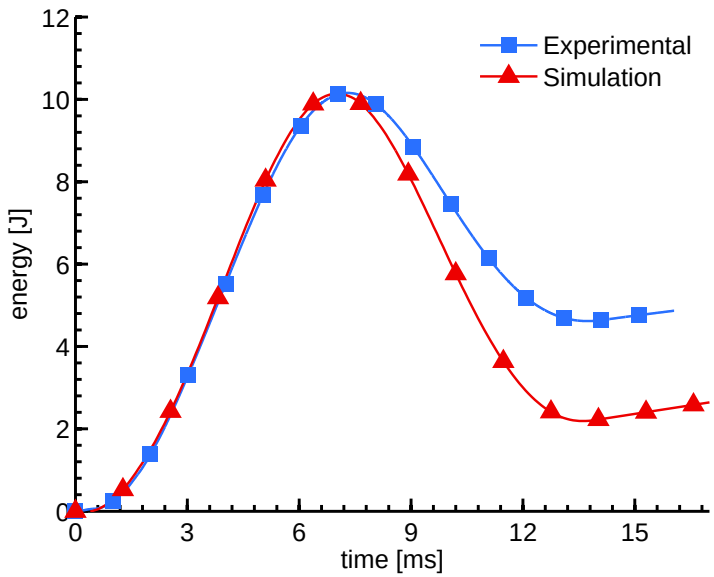

Figure 5: Variation of impactor energy with time in experiment and simulation

interaction is applied between two adjacent plies. Mode-I, II and III fracture energies are assigned to these cohesive surfaces which are used as governing parameters for the propagation of interlaminar damage. The inter-laminar damage initiation criteria is defined based on maximum nominal stress at the mating surfaces of the adjacent plies. As soon as the damage starts, a damage variable comes into the picture which can be represented as function of fracture energies. Fig. 4 shows the force-time and Fig. 5 shows the energy-time plots at 11 J impact energy. The force-time history comparison shows the overall good match between simulations and experiments. It is evident from the plots that simulation and experimental force time history results match very closely during pre-rebound phase. It is also observed that the during rebound phase the predictions of force-time history results from simulations show a slightly stiffer behavior which is also found in terms of mismatch in the energy-time history results during that phase. Although the simulations show lesser energy dissipation than experiments but

still the effect of these is found very minimal on force histories. It is anticipated that this mismatch can be reduced by increasing the number of partitions per phase for the reduced order homogenization.

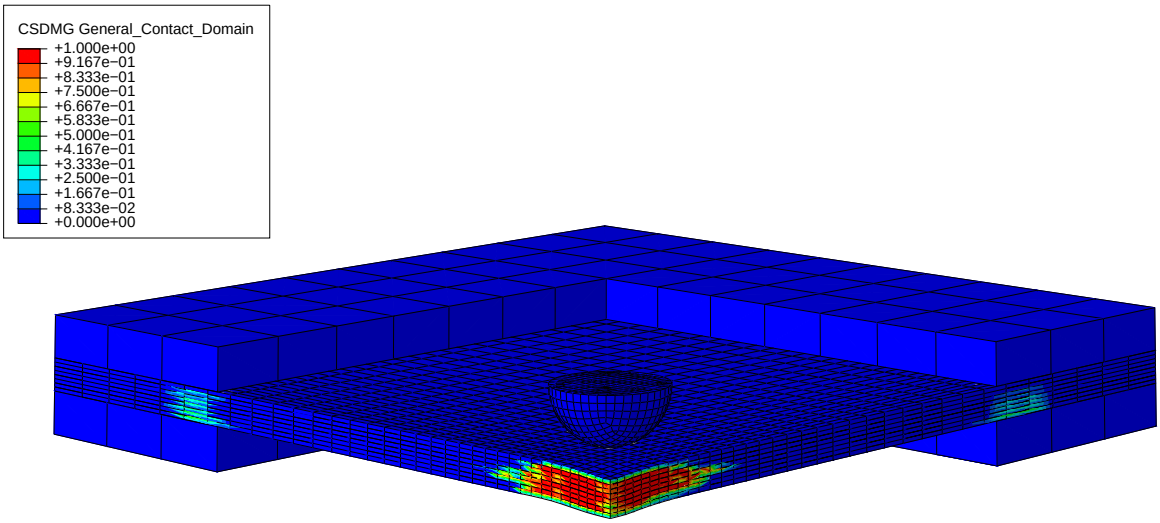

(a)

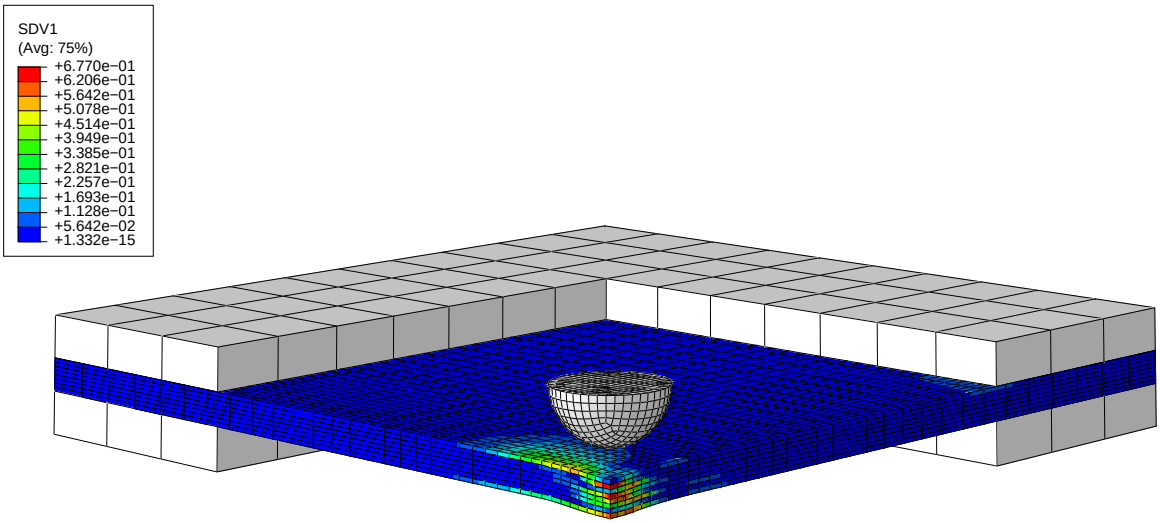

(b)

Figure 6: Contour plots for (a) Interlaminar damage and (b) Matrix damage

Damage occurred in the laminate in the form of delamination beneath the point of impact and more spread out matrix cracking. The damage areas due to impact yield map shown in Fig. 6. At first threshold matrix cracking occurs leading to softening and subsequent drop in force. This damage is due to matrix cracking and hence material softening causes sudden decrease in contact force. Fig. 6 also shows the comparison of interlaminar and matrix damage area and shows that interlaminar damage is major mode of failure. In the contour plot shown in Fig. 6 the blue region corresponds to $\Omega = 0$ where as red region indicates $\Omega = 1$. No fiber damage is observed in the present case.

Permanent deformation from simulation on the impact side is checked as shown in Fig. 7. Inelastic strain can be attributed as combined effect of matrix plasticity and damage.

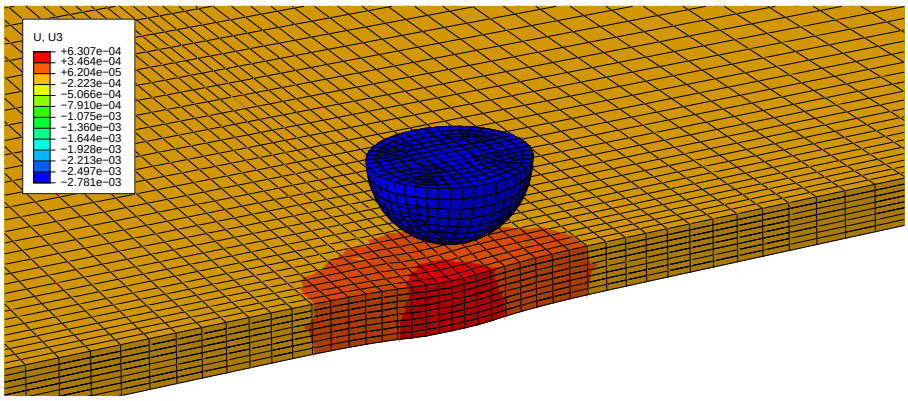

Figure 7: Contours of numerically predicted permanent deformations. The units of U3 are in m.

7 CONCLUSIONS

This paper presented the multiscale formulation which includes plasticity and damage effects for the fiber reinforced polymer composites. For microscale modeling, the constituents were tested for the determination of material data which was reproduced numerically by selecting the appropriate material models available in literature. These material models were further used for RVE simulations which was replaced with equivalent homogeneous material. For macroscale validation of the proposed formulation, drop weight impact tests were performed. The experimental data were obtained in terms of force-time history and energy-time history. Simulation was performed at the macroscale using the proposed model and results show a good match with the experimental and simulation results. In the end, permanent deformations predicted by the simulation was presented and the ability of the model to capture inelastic effects was demonstrated.

References

[1] Ram Raghava, Robert M Caddell, and Gregory SY Yeh. The macroscopic yield behaviour of polymers. *Journal of Materials Science*, 8(2):225–232, 1973.

[2] AS Wronski and M Pick. Pyramidal yield criteria for epoxides. *Journal of Materials Science*, 12(1):28–34, 1977.

[3] B Fiedler, M Hojo, S Ochiai, K Schulte, and M Ando. Failure behavior of an epoxy matrix under different kinds of static loading. *Composites Science and Technology*, 61(11):1615–1624, 2001.

[4] ALJTR Matzenmiller, J Lubliner, and RL Taylor. A constitutive model for anisotropic damage in fiber-composites. *Mechanics of materials*, 20(2):125–152, 1995.

[5] Prasanna Kumar Ilankeeran, Preetamkumar M Mohite, and Sudhir Kamle. Axial tensile testing of single fibres. 2012.

[6] Justin D Littell, Charles R Ruggeri, Robert K Goldberg, Gary D Roberts, William A Arnold, and Wieslaw K Binienda. Measurement of epoxy resin tension, compression, and shear stress–strain curves over a wide range of strain rates using small test specimens. *Journal of Aerospace Engineering*, 21(3):162–173, 2008.